DUBLINE: A DEEP UNFOLDING NETWORK FOR B-LINE DETECTION IN LUNG ULTRASOUND IMAGES

Tianqi Yang[1] *Nantheera Anantrasirichai*[1] *Oktay Karakuş*[2] *Marco Allinovi*[3]
Hatice Ceylan Koydemir[4,5] *Alin Achim*[1]

[1] Visual Information Lab, University of Bristol, Bristol, UK
[2] School of Computer Science and Informatics, Cardiff University, Cardiff, UK
[3] Nephrology, Dialysis and Transplantation, Careggi University Hospital, Florence, Italy
[4] Department of Biomedical Engineering, Texas A&M University, USA
[5] Center for Remote Health Technologies and Systems, Texas A&M Engineering Experiment Station, USA

ABSTRACT

In the context of lung ultrasound, the identification of B-lines, which serve as indicators of interstitial lung disease and pulmonary edema, holds immense significance in clinical diagnosis. Presently, although vision-based automatic B-line detection techniques have emerged, their performance remains suboptimal. This paper introduces a novel approach, framing B-line detection as an inverse problem through the deep unfolding of the Alternating Direction Method of Multipliers. By leveraging the capabilities of deep neural networks and model-based methods, this methodology addresses the challenges associated with data labeling and model training in lung ultrasound image analysis. Our primary aim is to significantly augment diagnostic precision while maintaining efficient real-time capabilities. The experiment on 34 patients demonstrates that the proposed method outperforms traditional model-based approaches, achieving a 10.6% higher F_1 score and running over 90 times faster, underscoring its potential for real-time clinical utility.

***Index Terms*—** deep unfolding, ADMM, lung ultrasound, line detection, inverse problem

1. INTRODUCTION

Lung ultrasound has emerged as an effective diagnostic tool for various pulmonary conditions. Techniques for analysing lung ultrasound images have been blooming in recent years [1]. One key finding in lung ultrasound (LUS) is the presence of B-lines, which appear as laser-like vertical hyperechoic reverberation artefacts originating from the pleural line. B-lines are indicators of the interstitial syndrome and are useful for the diagnosis of conditions like pneumonia and pulmonary edema, and have also been shown to correlate with the volume of extravascular lung water [2]. Thus, accurate detection of B-lines allows non-invasive evaluation of pulmonary edema and other conditions involving interstitial syndromes.

In previous efforts to automatically detect B-lines, various techniques were employed. Hand-crafted image processing techniques, like polar reformatting and thresholding, were used by Brattain et al. [3]. Anantrasirichai et. al. first posed line detection as an inverse problem [4, 5], where a B-mode LUS image is converted to a representation of radius and orientation in the Radon domain. The inverse problem is then solved using the alternating direction method of multipliers [6]. The method was further developed for evaluating COVID-19 patients by Karakus et. al. [7], whereby improved performance was achieved by regularising the solution using the Cauchy proximal splitting algorithm [8].

With the advent of deep learning, convolutional neural networks (CNN) have been applied for robust B-line detection. Van Sloun and Demi [9] applied a CNN with gradient-based class activation mapping [10] for B-line detection in single LUS frames. Alternatively, Baloescu et. al. [11] used a relatively shallow custom-made model architecture with 3-D filters for B-line assessment in a supervised manner. To extract better features across the video, Kerdegari et. al. [12] combined the long-short-term memory network and spatiotemporal attention mechanism to achieve B-line localisation. Our own work in [13] employed contrastive learning to investigate the representation of B-lines in an unsupervised manner. This was followed by fine-tuning on a limited labelled dataset, resulting in a significant reduction in the need for manual annotations.

In this paper, we propose a novel framework for B-line detection that leverages the advantages of model-based methods, eliminating the need for labelled data, and the fast inference capabilities of deep learning to enable real-time operation. Specifically, we adopt deep unfolding [14] to achieve rapid convergence by training a feedforward neural network to approximate iterative algorithms, namely the Alternating Direction Method of Multipliers (ADMM), speeding up the

e-mail: tianqi.yang@bristol.ac.uk

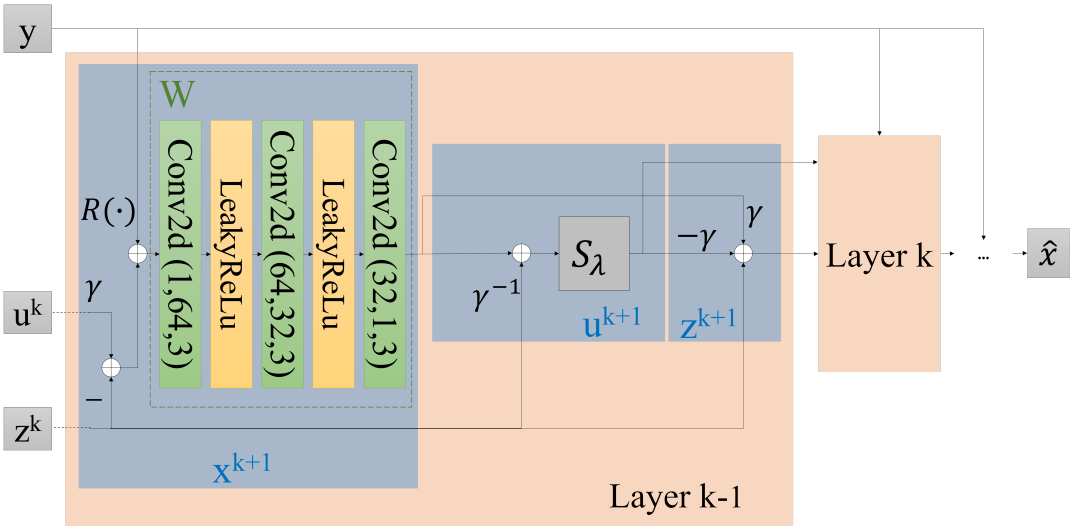

Fig. 1. Diagrammatic representation of DUBLINE. Trainable parameters are coloured in green.

optimisation for real-time applications. The design of the deep unfolded network (DUBLINE) for B-line detection in lung ultrasound was inspired by [4], and the architecture is shown in Fig.1, where a CNN is used to replace the complex Radon transform computations in the variable update steps.

2. METHODOLOGY

2.1. Line artefact model

The line artefact in the noisy ultrasound images can be modelled in terms of its inverse Radon transform as

$$y = R^{-1}x + n, \tag{1}$$

where y is the observed ultrasound image, x is the line represented by a distance r from the centre of y and a orientation ω from the horizontal axis of the image. R and R^{-1} represent the Radon transform and its inverse, respectively whilst n refers to the additive noise. In a general formulation without the noise, the Radon transform is described as in Eq.2, where $\delta(\bullet)$ is the delta function.

$$x = \int_{\mathbb{R}^2} y(i,j)\delta(r - icos\omega - jsin\omega)didj. \tag{2}$$

Using l_1 regularisation for sparsity, the estimation of lines can be found by solving the following optimisation problem with α being the regularisation constant:

$$\hat{x} = \arg\min_x \left\{ \frac{1}{2} \left\| y - R^{-1}x \right\|_2^2 + \alpha \left\| x \right\|_1 \right\}. \tag{3}$$

where discrete operators R and R^{-1}.

2.2. Optimisation problem

The problem in Eq.3 can be solved by employing ADMM [6], which is a variant of the augmented Lagrangian scheme that uses partial updates for the dual variables, so that Eq.3 is equivalent to

$$\begin{aligned} &\text{minimize} \quad \frac{1}{2} \left\| y - R^{-1}x \right\|_2^2 + \alpha \left\| u \right\|_1, \\ &\text{subject to} \quad x - u = 0. \end{aligned} \tag{4}$$

Then the augmented Lagrangian for Eq.4 is

$$\mathcal{L}_\gamma = \frac{1}{2} \left\| y - R^{-1}x \right\|_2^2 + \alpha \left\| u \right\|_1 + z^T(x-u) + \frac{\gamma}{2} \left\| x - u \right\|_2^2, \tag{5}$$

where z is the Lagrange multiplier, and z^T indicates the transpose of z. For penalty parameter $\gamma > 0$, the optimisation problem in Eq.4 can be solved by the iterative scheme of ADMM as stated in Eq.6 to 9.

Neural network formulation: The three-step iteration in Eq.6 to 9 can be formulated as a neural network, where the number of layers corresponds to the iteration counter in the traditional ADMM algorithm.

For updating x, the problem is solved as

$$\begin{aligned} x^{k+1} &= \arg\min_x \frac{1}{2} \left\| y - R^{-1}x \right\|_2^2 + (z^k)^T(x - u^k) \\ &\quad + \frac{\gamma}{2} \left\| x - u^k \right\|_2^2, \\ &= ((R^{-1})^T R^{-1} + \gamma I)^{-1}((R^{-1})^T y + \gamma u^k - z^k), \\ &= W_\theta(y, u^k, z^k). \end{aligned} \tag{6}$$

where k is an internal iteration counter, I denotes the identity matrix, W_θ denotes a CNN with 3 convolutional layers and LeakyReLu being the activation function. θ represents its parameters. In this paper, we use *radon_transformation*

functions[1] to construct R and R^{-1}. $(R^{-1})^T$ serves as the forward Radon projection.

For updating u, we have

$$\begin{aligned} u^{k+1} &= \arg\min_u \frac{\alpha}{\gamma}\|u\|_1 + \frac{1}{2}\left\|x^{k+1} - u + \frac{z^k}{\gamma}\right\|_2^2, \\ &= S_\lambda(x^{k+1} + \frac{z^k}{\gamma}). \end{aligned} \tag{7}$$

where $S_\lambda(\bullet)$ is a soft thresholding described in Eq.8 with a threshold of λ

$$S_\lambda(a) = sign(a)\max(|a| - \lambda, 0), \tag{8}$$

In this work, we take the maximum absolute row sum as the threshold. Lastly, each iteration for updating z follows

$$z^{k+1} = z^k + \gamma(x^{k+1} - u^{k+1}). \tag{9}$$

Loss function: We train the network to maximise the structural similarity index measure (SSIM) between the reconstructed line structures and the input image, and therefore the loss function is

$$L = (1 - SSIM(R^{-1}\hat{x}, y)). \tag{10}$$

Considering the nature of our problem, instead of other practical loss functions like MSE (regression), or cross-entropy (classification), we choose to promote SSIM thanks to its (i) artefact reduction capabilities, and (ii) robustness to common image degradations such as noise, or blurring. Ultrasound imagery and B-line detection are both suitable for the utilisation of SSIM due to aforementioned reasons and we leave the exploration of other loss functions for future work.

2.3. B-line detection

The B-line detection procedure in this paper aligns with [5], which detects the lines in the Radon domain using the local maxima technique. To reduce the influence of skin and muscle, the top part of the image is dimmed. The procedure starts with detecting the pleural line in the restored $\hat{x}$ within the angle $\Theta_h \in [90° \pm 5°]$ ($0°$ starts from the x axis). Then, the A-lines - physiological horizontal lines below the pleural line - are detected by using the same range of angles. The B-lines are detected at $\Theta_v \in [\pm 15°]$. Any vertical artefacts over-passed by an A-line are removed and all detected vertical lines that originate from the same pleural line point are counted as a single B-line.

3. EXPERIMENTAL RESULTS

Dataset and pre-processing: The data was obtained from the Nephrology, Dialysis and Transplantation, Careggi University Hospital, Florence, Italy. We trained the network on unlabeled lung ultrasound images. We used 1000 images as our training set and 122 images as the test set, from 34 patients. In the test set, there are 34 images with 0 B-lines, 43 with 1, 21 with 2, 20 with 3, and 4 with 4. LUS evaluations were performed whilst patients attended for regular haemodialysis, using an ultrasound machine (MyLab Class C-Esaote®, Genoa, Italy) with a 6–18 MHz linear probe. The ground truth was provided by a physician with long-term expertise in LUS. All the images were resized to 256×256 pixels.

Experimental setup: As we are specifically interested in the line structures in the lung ultrasound images, in DUBLINE, we implemented the Radon transform with the angle Θ_v and Θ_h as stated in the previous section. We set α and γ equal to 1 and the initial learning rate to 10^{-4} after a trial-error step. The learning rate decays every 10 epochs. The output of the network is acquired by comparing the reconstructed images and taking the maximum value of each pixel. We also evaluated DUBLINE for the number of layers of the unfolded network ranging from 2 to 10. The networks are all trained for 20 epochs. The training procedure is depicted in Fig.2. The network is implemented in PyTorch and trained on Nvidia Geforce RTX 3090. The method in [5] is reproduced using 12th Gen Intel® Core™ i7-12700 2.10 GHz.

Results Analysis: We compare the performance with the method in [5] following the same detection process and adjusted the parameters accordingly to improve the detection performance. Our assessment focused on various performance metrics, including true positives (TP), false positives (FP), false negatives (FN), precision, recall, and the F_1 score. The results of this comparison are summarized in Table 1, where "DU" denotes our proposed DUBLINE method and the best result obtained is in bold. When assessing the model's performance across different numbers of iterations, it becomes evident that training DUBLINE with more than 2 layers consistently outperforms the baseline method [5] across all the metrics. This can be attributed to the traditional method typically requiring more than 2 iterations in the ADMM algorithm to meet the stopping criteria. As a result, the deep unfolded network necessitates at least 3 layers to achieve equal or superior performance to the method outlined in [5]. Further examination of layer numbers 3 through 10 reveals that DUBLINE exhibits higher TP rates and lower FN rates, leading to a significant improvement of at least 10.5% in recall for the detection task. The best-performing is observed at layer8, which yields the highest TP count (100) and the lowest FN count (61), resulting in a notable 10.6% enhancement in the F_1 score. Across the board, the number of FPs is reduced, with the most substantial reduction being 13 when compared to the baseline. While there are exceptions at layer3 and layer9, the precision scores are still improved by 4.9% and 6.4%, respectively.

Fig.3 shows some examples of B-line detection results. When the green lines fall within half of the ground truth box

[1] https://github.com/drgHannah/Radon-Transformation/tree/main

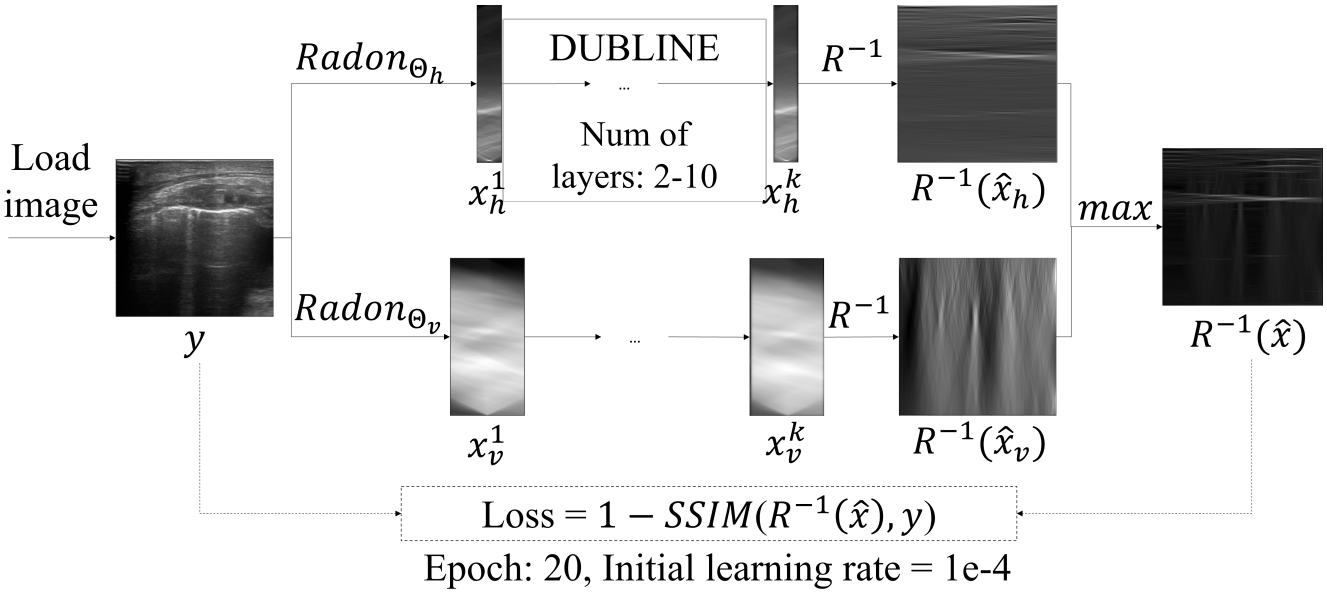

Fig. 2. Training procedure of DUBLINE.

width centring at the centre line of the ground truth box, they are counted as TP. If the green lines fall outside of this range, they are counted as FP. When there is no green line within the yellow box, it is counted as an FN. As shown in the examples, compared to the method described in [5], the proposed method detects more correct B-lines and significantly improves the accuracy of their detected positions. However, the proposed method exhibits relatively poor differentiation between the true B-lines and the bright vertical lines that only look similar to B-lines, causing FPs to often occur at the positions of bright vertical artefacts. In cases when the pleural line is darker than the horizontal artefacts above it, the detected position of the pleural line is likely to be biased, resulting in the starting point of the B-lines being higher than the actual position.

We highlight the time efficiency of the DUBLINE by comparing it with that of the method in [5]. The execution time per image of the DUBLINE is only 0.0186 seconds, whereas the average speed of the traditional ADMM is 1.6803 seconds per image. The unfolded algorithm significantly improves the speed by more than 90 times with less than 0.5 seconds to process 24 frames in a real-time video.

4. CONCLUSION

In this paper, we propose a fast and lightweight method based on a deep unfolded ADMM algorithm to tackle B-line detection in lung ultrasound as an inverse problem, with the ultimate goal of achieving completely unsupervised real-time B-line detection. Compared to the traditional model-based method, the proposed approach shows an improvement in precision, recall, accuracy, F_1 score, and time efficiency. However, the limitation still exists in the detection procedure. Future works will explore possible unsupervised approaches that can further enhance the accuracy and robustness of B-line detection.

Table 1. Detection results from different settings

		TP	FP	FN	Precision	Recall	F1
[5]		74	166	87	0.308	0.46	0.369
DU	layer2	61	154	100	0.284	0.379	0.324
	layer3	94	169	67	0.357	0.584	0.443
	layer4	93	158	68	0.371	0.578	0.451
	layer5	91	157	70	0.367	0.565	0.445
	layer6	97	158	64	0.38	0.602	0.466
	layer7	93	**153**	68	0.378	0.578	0.457
	layer8	**100**	160	**61**	**0.385**	**0.621**	**0.475**
	layer9	99	167	62	0.372	0.615	0.464
	layer10	98	162	63	0.377	0.609	0.466

5. ETHICAL STATEMENT

The study protocol conformed to the Declaration of Helsinki and was approved by a local research ethics committee (study approval number 18217/OSS). Informed consent was obtained from all subjects involved in the study.

6. REFERENCES

[1] T. Yang, O. Karakuş *et al.*, "Current advances in computational lung ultrasound imaging: a review," *IEEE Trans. on Ultrason., Ferroelect., and Freq. Control*, 2022.

[2] M. Allinovi, M. Saleem *et al.*, "Lung ultrasound: a novel technique for detecting fluid overload in children on dialysis,"

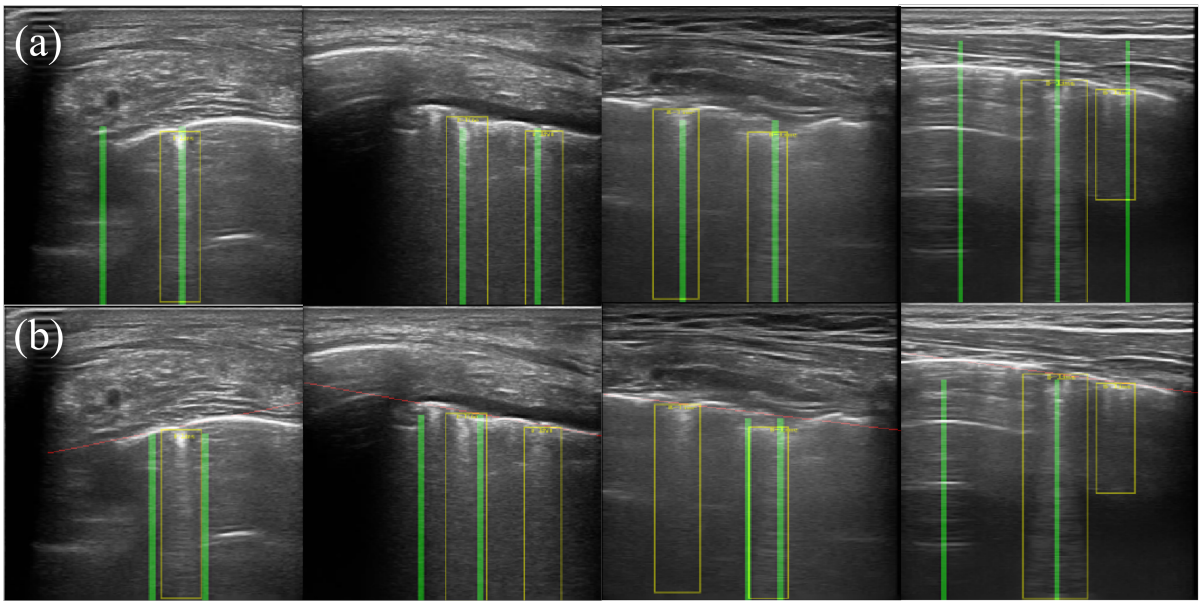

Fig. 3. B-line detection results. (a) is the results of the DUBLINE and (b) is the results of [5]. The yellow boxes are the bounding boxes of the ground truth. The green lines are the detected B-lines.

Nephrology Dialysis Transplantation, vol. 32, no. 3, pp. 541–547, 2017.

[3] L. J. Brattain, B. A. Telfer *et al.*, "Automated B-line scoring on thoracic sonography," *J. of Ultrasound in Medicine*, vol. 32, no. 12, pp. 2185–2190, 2013.

[4] N. Anantrasirichai, M. Allinovi *et al.*, "Automatic B-line detection in paediatric lung ultrasound," in *2016 IEEE Int. Ultrason. Symposium (IUS)*. IEEE, 2016, pp. 1–4.

[5] N. Anantrasirichai, W. Hayes *et al.*, "Line detection as an inverse problem: application to lung ultrasound imaging," *IEEE Trans. on Med. Imag.*, vol. 36, no. 10, pp. 2045–2056, 2017.

[6] S. Boyd, N. Parikh *et al.*, "Distributed optimization and statistical learning via the alternating direction method of multipliers," *Found.s and Trends® in Mach. Learn.*, vol. 3, no. 1, pp. 1–122, 2011.

[7] O. Karakuş, N. Anantrasirichai *et al.*, "Detection of line artifacts in lung ultrasound images of Covid-19 patients via non-convex regularization," *IEEE Trans. on Ultrason., Ferroelect., and Freq. Control*, pp. 2218–2229, 2020.

[8] O. Karakuş, P. Mayo *et al.*, "Convergence guarantees for non-convex optimisation with Cauchy-based penalties," *IEEE Trans. on Signal Process.*, vol. 68, pp. 6159–6170, 2020.

[9] R. J. Van Sloun and L. Demi, "Localizing B-lines in lung ultrasonography by weakly supervised deep learning, in-vivo results," *IEEE J. of Biomed. and Health Inform.*, pp. 957–964, 2019.

[10] R. R. Selvaraju, M. Cogswell *et al.*, "Grad-Cam: Visual explanations from deep networks via gradient-based localization," in *Proceedings of the IEEE Int. Conf. on Comput. Vision*, 2017, pp. 618–626.

[11] C. Baloescu, G. Toporek *et al.*, "Automated lung ultrasound B-line assessment using a deep learning algorithm," *IEEE Trans. on Ultrason., Ferroelect., and Freq. Control*, pp. 2312–2320, 2020.

[12] H. Kerdegari, N. T. H. Phung *et al.*, "B-line detection and localization in lung ultrasound videos using spatiotemporal attention," *Appl. Sci.*, p. 11697, 2021.

[13] T. Yang, N. Anantrasirichai *et al.*, "A semi-supervised learning approach for B-line detection in lung ultrasound images," *IEEE Int. Symposium on Biomed. Imag.*, pp. 1–5, 2022.

[14] A. Balatsoukas-Stimming and C. Studer, "Deep unfolding for communications systems: A survey and some new directions," in *2019 IEEE Int. Workshop on Signal Process. Syst. (SiPS)*. IEEE, 2019, pp. 266–271.